

A COMPARATIVE STUDY OF THE PHYSICO-CHEMICAL PROPERTIES AND METHYLENE BLUE ADSORPTION BEHAVIOUR OF FLY ASH, NANO-OXIDES AND THE COMPOSITE MATERIALS OF NANO-OXIDES AND FLY ASH

Olushola S. Ayanda^{1*} --- Olalekan S. Fatoki² --- Folahan A. Adekola³ --- Bhekumusa J. Kimba⁴ --- Jimoh O. Tijani⁵ --- Leslie F. Petrik⁶

¹Environmental and Nano Science Research Group, Department of Chemistry, University of the Western Cape, Bellville, South Africa,
²Department of Chemistry, Faculty of Applied Sciences, Cape Peninsula University of Technology, Bellville, South Africa

^{3,4}Department of Chemistry, Faculty of Applied Sciences, Cape Peninsula University of Technology, Bellville, South Africa

⁵Department of Chemistry, University of Ilorin, Ilorin, Nigeria

⁶Environmental and Nano Science Research Group, Department of Chemistry, University of the Western Cape, Bellville, South Africa

ABSTRACT

In this present study, composite materials involving fly ash produced from coal combustion and nano-oxides were prepared. The nature, morphology and properties of the precursors and the composite materials were determined by modern instrumental analytical techniques such as carbon, nitrogen and hydrogen (CNH) analysis, Brunauer–Emmett–Teller (BET) surface area and porosity analysis, scanning and transmission electron microscopy, and x-ray diffraction. Particle size distribution, ash content, pH and point of zero charge were also investigated. The adsorption kinetics of methylene blue (MB) onto these adsorbents was examined. Experimental results showed that the composition of fly ash and nano-oxides contributed to the development of intergranular voids and crevices with high surface and micropore areas that enhanced the adsorption of MB from an aqueous solution. The adsorption of MB onto the precursors and the composite materials follow the pseudo-second order kinetic model.

Keywords: Fly ash, Nano-oxides, nFe₃O₄/fly ash, nSiO₂/fly ash, nZnO/fly ash, Methylene blue, Adsorption, Kinetics.

Contribution/ Originality

This study contributes in the existing literature that fly ash, nano-oxides and composite materials can be used for the remediation of organic pollutants from wastewaters. This study involves the preparation of composite materials from fly ash and nano-oxides, characterization, and demonstration of the methylene blue adsorption utilization potential. The method used for the preparation of the composites is simple, modern instrumental analytical techniques were used

for the characterization, and a standard method used to simulate organic pollutants was used to assess the adsorption potential of precursors and composites.

1. INTRODUCTION

The increasing demand for energy throughout the world has led to an increase in the utilization of coal in power stations and, subsequently, in the production of large quantities of fly ash as a by-product. It has been estimated that coal-based thermal power plants annually generate more than 500 million tons of fly ash as a by-product of coal combustion [1]. At present, fly ash finds use in the cement and concrete building industry [2]. With only about 20-30 % of the generated fly ash being used as an additive in cement and concrete manufacture, the management of fly ash consequently becomes a global concern from environmental and economic points of view [3]. Fly ash typically consists of crystalline aluminosilicate, mullite and α -quartz along with trace amounts of calcium, magnesium, potassium, sodium and titanium oxides, depending on the nature of the coal burned. The particle size distribution patterns of the spherical shaped fly ash are in the range of 1 to 100 μm based on the processing condition [4, 5]. Due to the high silica and alumina content, fly ash can be transformed into zeolite-like crystalline materials by chemical treatment and could be used as adsorbents and ion exchangers in water and wastewater treatment [6, 7].

Several researchers have reported the application of fly ash as composites in reinforced glass and polymer matrix, composites with metals [8], and as catalyst supports [3, 9]. However, the industrial application of fly ash is limited by inherent factors such as its low whiteness values and low friction when untreated. For this reason, several surface modifiers and modifying technologies have been applied to fly ash in order to improve structural characteristics such as its surface area, pore volume, surface wetting, dispersiveness, pH, electricity, weathering resistance, gloss, antibacterial property, mechanical strength, stress and stiffness resistance, etc. [10]. The application of fly ash for the remediation of environmental pollutants has been widely reported [11-14]. We have also reported the application of fly ash, $n\text{Fe}_3\text{O}_4$ /fly ash composite, and $n\text{SiO}_2$ /fly ash composite for the adsorption of triphenyltin chloride from seawater [15, 16]. Nevertheless, it will also be of interest to report the detailed physico-chemical properties of these materials and investigate their methylene blue (MB) adsorption efficiencies.

MB remediation is a standard method used to simulate organic pollutants and was used to assess the adsorption potential of fly ash, nano-oxides and their composites. MB is a dye (Fig. 1) that is generally used for dyeing cotton, wool, and silk. Dyes are of great concern because of their extensive use, bio-recalcitrant properties and their toxic aromatic intermediates [17, 18]. MB can therefore cause eye burns in humans and animals, methemoglobinemia, cyanosis, convulsions, tachycardia, dyspnea, irritation to the skin and, if ingested, irritation to the gastrointestinal tract, nausea, vomiting, and diarrhoea [19].

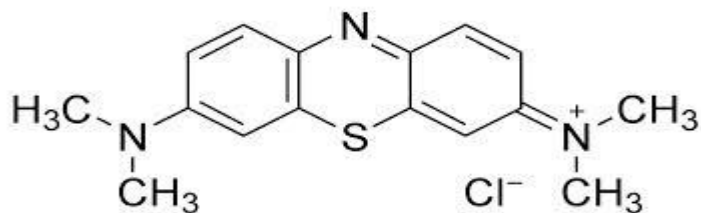


Fig-1. Methylene blue.

The aim of this study is, therefore, to compare the physico-chemical properties of fly ash, nano-oxides, $n\text{Fe}_3\text{O}_4$ /fly ash, $n\text{SiO}_2$ /fly ash and $n\text{ZnO}$ /fly ash composite materials using modern analytical techniques, followed by the demonstration of their MB adsorption utilization potential.

2. EXPERIMENTAL

2.1. Fly Ash, Nano-Oxides and Composites

The fly ash used in this study was obtained from the Matla Power Station, Mpumalanga, South Africa. Iron (II, III) oxide nano powder ($n\text{Fe}_3\text{O}_4$), silica nano powder ($n\text{SiO}_2$) and zinc oxide NanoGard ($n\text{ZnO}$) APS powder were purchased from Sigma Aldrich, USA. Methanol was purchased from Industrial Analytical, South Africa. Potassium bromide (KBr) and sodium nitrate (NaNO_3) were bought from Merck, Germany. The nano-oxides/fly ash composites in the ratio 1:1 were prepared [15] and MB dye (99.9% from Sigma Aldrich, USA) was used as an adsorbate in this work.

2.2. Instrumentation

The nature, morphology and properties of the fly ash, nano-oxides, and the composite materials were investigated and compared by the use of Euro Ea elemental analyser, scanning and transmission electron microscope, Tristar 3000 analyzer for surface area and porosity analysis, and x-ray diffractometer. The particle size distribution, ash content, pH, and point of zero charge were also considered.

2.2.1. CNH Analysis

A 3 mg solid sample in a sealed tin capsule was put into an auto sampler tray and loaded on Euro Ea elemental analyzer where the sample was combusted and analyzed for the percentage carbon, nitrogen and hydrogen contents.

2.2.2. Electron Microscopy

A small quantity of the sample spread on a thin layer of carbon glue on a stub was coated with carbon using carbon coater (Balzers model BSV 202) for 1 hr. The scanning electron micrographs (SEM) of the samples were viewed under an FEI™ scanning electron microscope (Nova Nano SEM 230). For the transmission electron micrograph (TEM), a few drops of 0.1 g of the samples homogeneously dispersed in 0.6 ml methanol for 30 seconds were placed on a carbon

coated copper grid and allowed to dry. The dried carbon coated copper grids were placed on a single tilt sample holder and were loaded on the Tecnai G² 20 transmission electron microscope.

2.2.3. Measurement of the Particle Size Distribution

Determination of the particle size distribution of nFe₃O₄, nSiO₂, and nZnO was carried out by the use of TEM, while SEM was used to determine the particle size distribution of fly ash. IMAGEJ software was used to determine the population and diameter of the various particles on the micrographs. The percentage population was therefore plotted against the diameter (nm).

2.2.4. pH Determination

Determination of pH was performed by gently boiling 50 mL of Milli-Q water in a flask containing 0.1 g of the samples for 5 min. The pH was measured after the solution was cooled to room temperature using a Mettler Toledo pH meter.

2.2.5. Point of Zero Charge (PZC) by Mass Titration

Increasing amounts of samples ranging from 0 to 2.0 g were added to 10 mL of 0.01 M NaNO₃ solution. The resulting pH of each suspension was measured after 24 hr. The pH plateau for the highest concentrations of solid in a successful series of mass titrations was taken as the PZC of the materials [20].

2.2.6. Determination of the Ash Content

A 0.1 g of the samples was measured into crucibles and heated in a muffle furnace (Carbolite Sheffied model LMF 4) at the high temperature of 600 ± 1 °C for 4 hr. After ashing, the samples were withdrawn from the furnace, allowed to cool in a desiccator and were reweighed. The ash content of the precursors and the composites were calculated by Equation 1 and the experiment was carried out in triplicate.

$$\text{Ash content (\%)} = (W_3 - W_1) / (W_2 - W_1) \times 100 \quad (1)$$

where W_1 is the mass of crucible, W_2 is the mass of crucible + sample before ashing and W_3 is the mass of crucible + sample after ashing (W_3).

2.2.7. X-Ray Diffraction

The fly ash, nano-oxides and composites were subjected to x-ray diffraction analysis using a PAN-analytical PW 3830 diffractometer system with CuK α radiation. The diffractometer was operated at 40 kV and 25 mA for 1 hr over the range of 2 θ from 0° to 80°. The phase identification of all the samples was obtained and the diffractogram compared.

2.2.8. BET Surface Area and Porosity Determination

The specific surface area of the precursors and composites was obtained using a Tristar 3000 analyzer with N₂ adsorption at - 196 °C. The samples were first degassed at 200 °C for 4 hr prior to the analysis.

2.3. Adsorption Procedure

A 10 mg/L MB solution (pH 6.8) was prepared by dissolving the appropriate amount of MB in 1000 mL of distilled water. Adsorption was performed in a 250 mL flask containing 100 mL of MB solution. 0.5 g of adsorbent was added to the flask on a shaker (200 rpm) and a supernatant solution was taken at 5, 10, 20, 40, and 80 minute contact times at a temperature of 25 °C. The concentrations of MB in the supernatant solutions before and after adsorption were determined using a GBC 920 uv-vis spectrophotometer at a wavelength of 665 nm. All experiments were carried out in triplicate and only the mean values were reported. It should also be noted that the effect of pH on the adsorption efficiency of MB unto the adsorbents was not considered in this study. The amount of MB adsorbed onto the adsorbents was calculated by mass balance. The pseudo-second order (Equation 2) equation was used to model the kinetic data.

$$\frac{t}{q_t} = \frac{1}{k_2 q_e^2} + \frac{1}{q_e} (t) \quad (2)$$

where q_e is the equilibrium concentration of MB and k_2 is the pseudo second – order constant calculated from the slope and intercept of Equation 2, respectively. h_o which is equal to $k_2 q_e^2$ is the initial adsorption rate.

3. RESULTS AND DISCUSSION

3.1. CNH Content

Table 1 shows that the fly ash contained 1.54 % carbon, while the nitrogen and hydrogen content were below the detection limit. The nitrogen content of nFe₃O₄, nSiO₂ and nZnO were all below the detection limit; the hydrogen and carbon contents of nSiO₂ were each 0.76 %, while the hydrogen percentage content of nFe₃O₄ and nZnO were also below the detection limit. The nFe₃O₄/fly ash composite thus contained 0.55 % carbon, 1.0 % hydrogen and the nitrogen content was below the detection limit.

The nSiO₂/fly ash composite, on the other hand, contained 0.80 % carbon, 1.43 % hydrogen and the nitrogen content was below the detection limit, while the nZnO/Fly ash composite contained 0.79 % carbon, 1.07 % hydrogen content and the nitrogen content was also below the detection limit.

Table-1. Percentage carbon, nitrogen and hydrogen of the precursors and composite materials.

Adsorbents	% C	% N	% H
Fly ash	1.54	BD	BD
nFe ₃ O ₄	0.46	BD	BD
nSiO ₂	0.76	BD	0.76
nZnO	0.42	BD	BD
nFe ₃ O ₄ /fly ash	0.55	BD	1.00
nSiO ₂ /fly ash	0.80	BD	1.43
nZnO/fly ash	0.79	BD	1.07

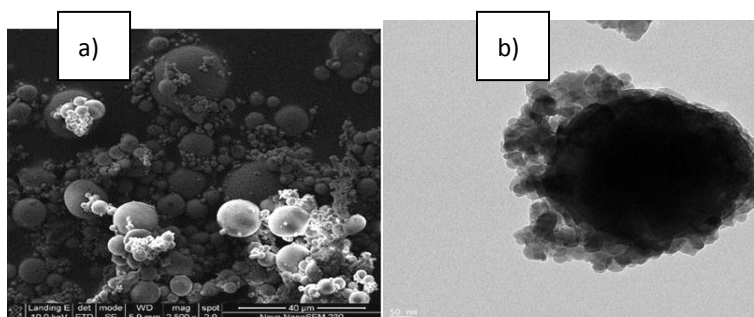
BD - Below detection of 0.001 wt%. Quality control - Acetalinide std. measured: C – 73.00 %, N - 10.85 % and H – 6.42%; Acetalinide std value: C – 71.10 %, N - 10.40 % and H – 6.70%.

The result showed that the carbon content of fly ash decreased by 64.29 %, 48.05 % and 48.70 % in the prepared nFe₃O₄/fly ash, nSiO₂/fly ash, and nZnO/fly ash composite, respectively. The nitrogen content in all the composites was below the detection limit. The hydrogen content percentage of nFe₃O₄, nSiO₂, and nZnO in their corresponding composites were raised to 1.00 %, 1.43 % and 1.07 %, respectively.

3.2. SEM and TEM Results

The SEM of fly ash (Fig. 2a) showed that each of the particles of Matla fly ash is spherical with smooth and regular surfaces. The size of the spheres was found to be 0.6 - 26.2 μm and the mean particle size was 3.2 ± 3.9 μm. The cracks of some of the spheres showed that the fly ash particles are hollow. The TEM of fly ash (Fig. 2b) presents agglomeration of different particle sizes. The fly ash particles manifested several size distributions and spherical shapes as shown in Fig. 2a and 2b.

The SEM of nFe₃O₄ (Fig. 2c) showed that nFe₃O₄ consists of agglomerated globules with irregular and rough surfaces. The micrograph showed that nFe₃O₄ is made up of particles of various sizes. The TEM of nFe₃O₄ (Fig. 2d) thus presents agglomeration of particle sizes ranging between 10.8 and 77.3 nm. The TEM showed that nFe₃O₄ is made up of various shapes including squares, spheres and hexagons. The mean particle size of nFe₃O₄ was 34.1 ± 13.7 nm.



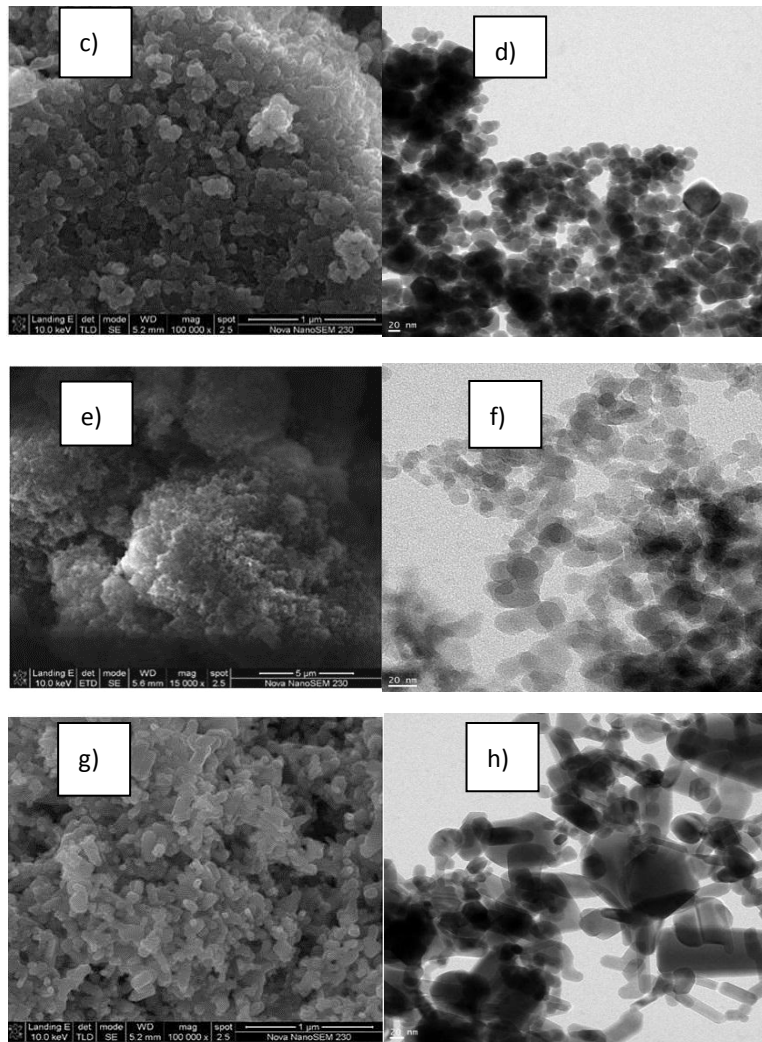


Fig-2. SEM and TEM of fly ash, $n\text{Fe}_3\text{O}_4$, $n\text{SiO}_2$, and $n\text{ZnO}$.

The SEM of $n\text{SiO}_2$ (Fig. 2e) showed that $n\text{SiO}_2$ exhibited agglomerated irregular surfaces with a large number of micropores and a few voids and crevices. The TEM of $n\text{SiO}_2$ (Fig. 2f) shows a bimodal distribution of particles size. This is in support of the result of [Gianina, et al. \[21\]](#) who reported the TEM of SiO_2 powder. The TEM also showed that the particle size of $n\text{SiO}_2$ ranges between 9.8 and 33.9 nm with a mean particle size of 19.3 ± 6 nm.

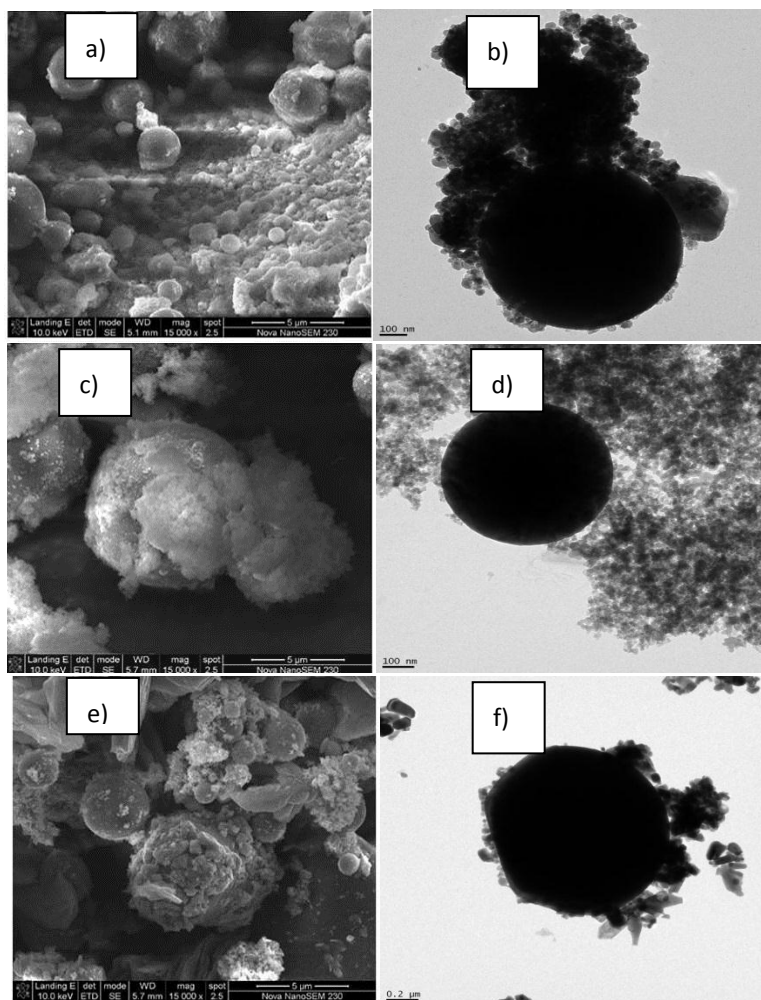


Fig-3. SEM and TEM of $n\text{Fe}_3\text{O}_4$ /fly ash, $n\text{SiO}_2$ /fly ash, and $n\text{ZnO}$ /fly ash composite.

The SEM and TEM of $n\text{ZnO}$ (Fig. 2g and 2h) showed that $n\text{ZnO}$ particles consist of uniform granules and more regular surfaces. The TEM of $n\text{ZnO}$ (Fig. 2h) confirms the various shapes and sizes of $n\text{ZnO}$ particles, the shapes being spherical, rectangular, hexagonal and rod-like. The TEM of $n\text{ZnO}$ thus presents granules of particle sizes ranging from between 15.9 and 144.7 nm with a mean particle size of 53.5 ± 26.6 nm.

The SEM of $n\text{Fe}_3\text{O}_4$ /fly ash composite (Fig. 3a) showed an aggregated $n\text{Fe}_3\text{O}_4$ and fly ash particles. The figure also shows that the $n\text{Fe}_3\text{O}_4$ particles exhibited irregular surfaces whereas the fly ash retained its spherical and smooth surface. The TEM of $n\text{Fe}_3\text{O}_4$ /fly ash composite (Fig. 3b) showed an aggregate of spherical fly ash and $n\text{Fe}_3\text{O}_4$ with large crevices. The result also showed that the fly ash particles maintained their spherical morphology after preparation of the $n\text{Fe}_3\text{O}_4$ /fly ash composite.

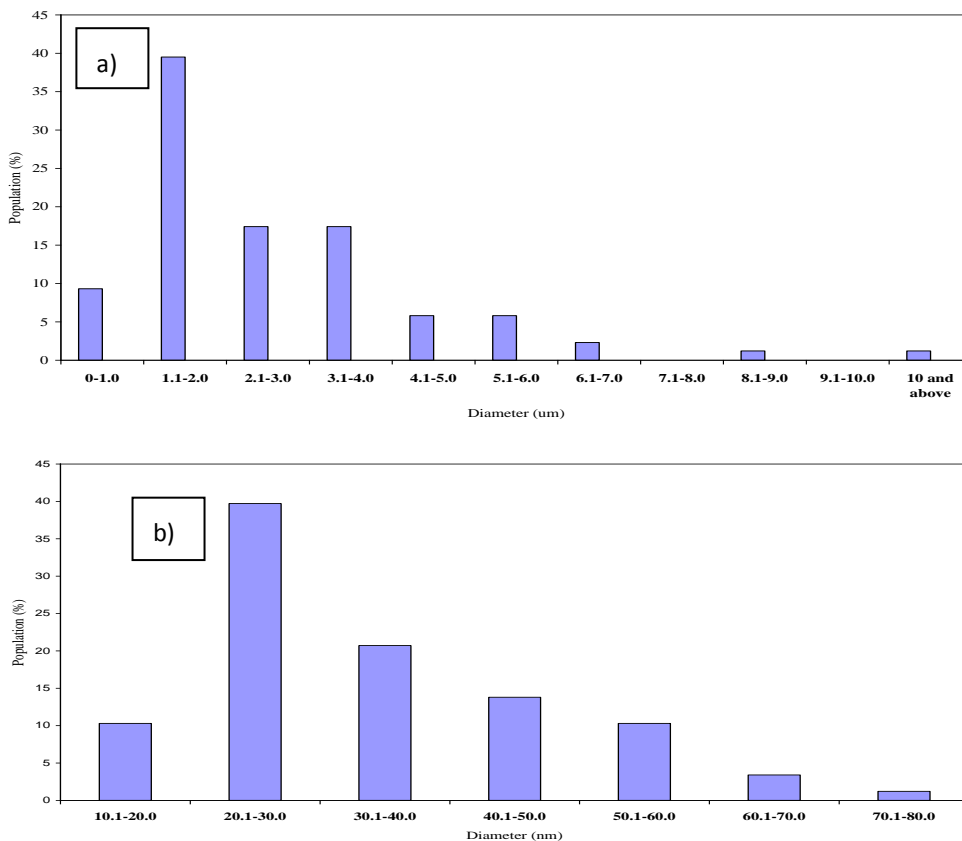
The SEM of $n\text{SiO}_2$ /fly ash composite (Fig. 3c) showed that the $n\text{SiO}_2$ with irregular surfaces and large number of micropores was deposited at various positions on the spherical surface of the

fly ash. The TEM of nSiO₂/fly ash composite (Fig. 3d) thus showed a highly porous nSiO₂ surrounding the spherical fly ash.

The SEM of nZnO/fly ash composite (Fig. 3e) showed that the fly ash and nZnO particles were clustered together with large intergranular voids and crevices present. The TEM of nZnO/fly ash composite (Fig. 3f) also confirmed a clustered nZnO/fly ash composite with intergranular voids and crevices. The SEM and TEM (Fig. 3e and 3f) showed that the fly ash and nZnO particles maintained their morphology after preparation of the nZnO/fly ash composite.

3.3. Particle Size Distribution

Fig. 4a shows that the particle size of fly ash ranges from 0.6 to 26.2 μm, the mean particle size is 3.2 μm, and the standard deviation is 3.9. The graph of the particle size distribution of fly ash showed that the fly ash mainly consisted of between 1.1 and 1.2 μm sized particles, however particles greater than 10 μm size were present but very minute in the sample.



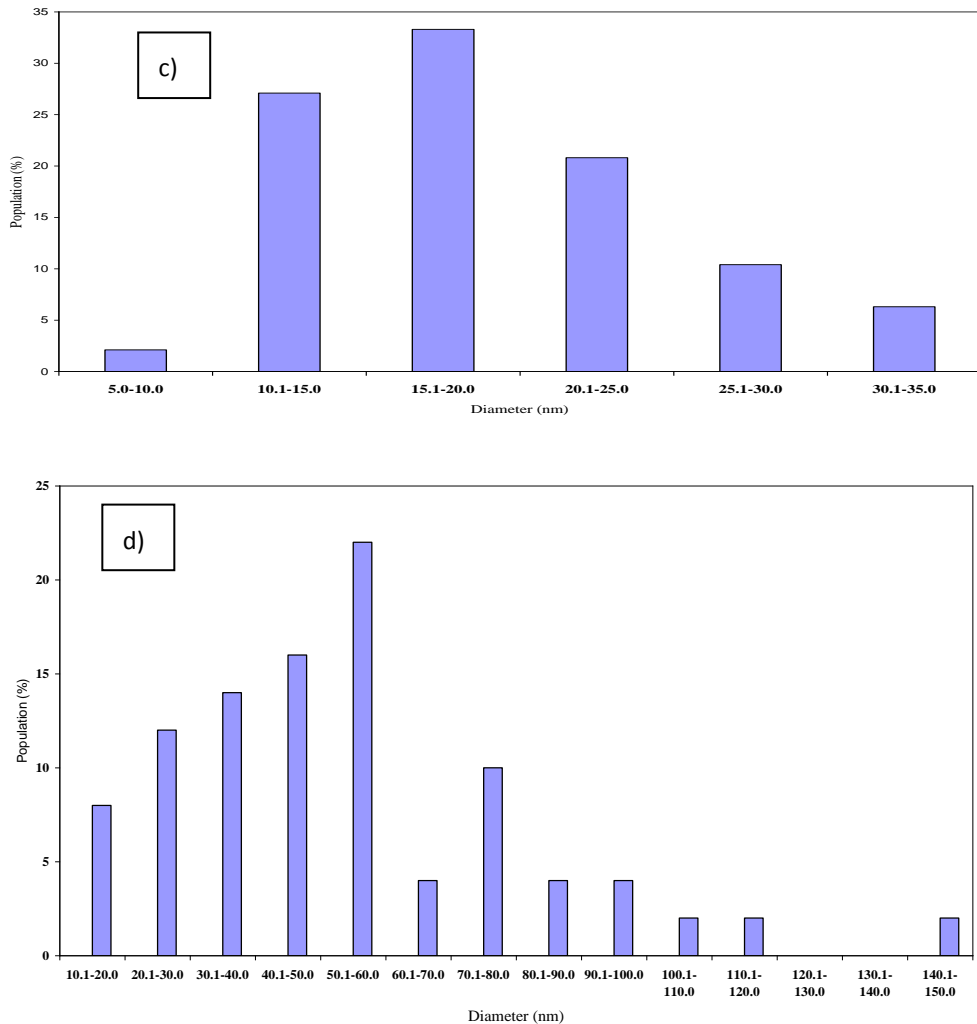


Fig-4. Particle size distribution of fly ash (a), nFe₃O₄ (b), nSiO₂(c) and nZnO (d).

Fig. 4b shows that the particle size of nFe₃O₄ is between 10.87 and 77.3 nm, the mean particle size is 34.1 nm, and a standard deviation of 13.7. The graph of the particle size distribution of nFe₃O₄ showed that the nFe₃O₄ is mostly between 20.1 and 30.0 nm particle sizes. Fig. 4c shows that the particle size of nSiO₂ ranges from 9.8 to 33.9 nm, the mean particle size is 19.3 nm and shows a standard deviation of 6. The graph showed that nSiO₂ is mostly distributed between 10.1 and 20.0 nm particle sizes. In Fig. 4d it can be seen that the particle size of nZnO is between 15.9 – 144.7 nm, the mean particle size is 53.5 and that there is a standard deviation of 26.6. The graph of the nZnO particle size distribution showed that this was slightly more evenly distributed, between 20.1 – 60.1 nm particle sizes. Many particles were found to be less than 40 nm in size while fewer particles were greater than 100 nm.

3.4. pH and PZC Measurement

Fig. 5 shows that the preparation of $n\text{Fe}_3\text{O}_4$ /fly ash composite using fly ash (pH = 10.70) and $n\text{Fe}_3\text{O}_4$ (pH = 5.95) as precursors resulted in a $n\text{Fe}_3\text{O}_4$ /fly ash composite of pH 3.54, the pH being lower than the pH of fly ash by 66.9 % and lower than the pH of $n\text{Fe}_3\text{O}_4$ by 40.5 %. The preparation of $n\text{SiO}_2$ /fly ash composite using fly ash (pH = 10.70) and $n\text{SiO}_2$ (pH = 5.53) as precursors resulted in a $n\text{SiO}_2$ /fly ash composite of pH 3.48; the pH was lower than the pH of fly ash by 67.5 % and also lower than pH of $n\text{SiO}_2$ by 37.1 %, while the preparation of $n\text{ZnO}$ /fly ash composite using fly ash (pH = 10.70) and $n\text{ZnO}$ (pH = 6.71) as precursors resulted in a $n\text{ZnO}$ /fly ash composite of pH 6.96; the pH was lower than the pH of fly ash by 34.9 % but higher than the pH of $n\text{ZnO}$ by 3.59 %. The result showed that the pH of the composites is a function of the pH of each of the component precursors that made up the composite materials.

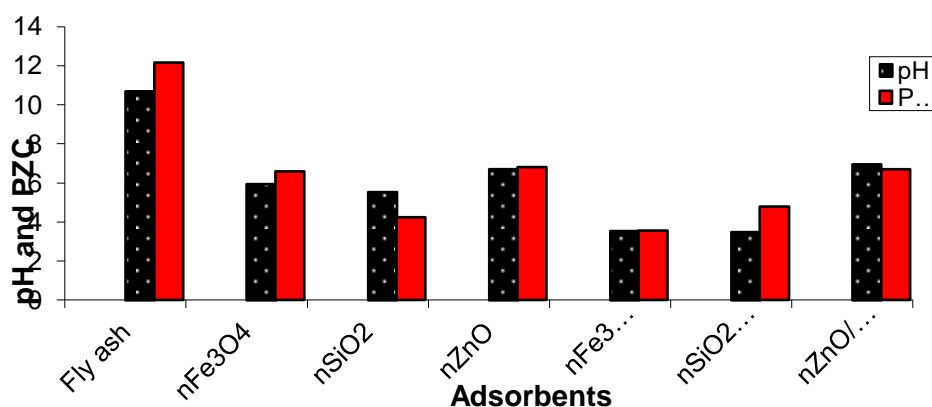


Fig-5. pH and PZC of fly ash, nano-oxides and composites.

Fig. 5 also shows that the PZC of fly ash, $n\text{Fe}_3\text{O}_4$, and $n\text{Fe}_3\text{O}_4$ /fly ash composite are 12.17, 6.58 and 3.57, respectively. The PZC of $n\text{Fe}_3\text{O}_4$ /fly ash composite was lower than the PZC of fly ash by 70.67 % and lower than the PZC of $n\text{Fe}_3\text{O}_4$ by 45.74 %. The PZC of $n\text{SiO}_2$ and $n\text{SiO}_2$ /fly ash composite was 4.25 and 4.80, respectively. The PZC of $n\text{SiO}_2$ /fly ash composite is therefore lower than the PZC of fly ash by 60.56 % but higher than the PZC of $n\text{SiO}_2$ by 11.46 %. The PZC of $n\text{ZnO}$ /fly ash composite is 6.70. The PZC value is lower than the PZC of fly ash (12.17) and lower than the PZC of $n\text{ZnO}$ (6.80) by 44.95 and 1.47 %, respectively. It can therefore be concluded that the presence of nano-oxides in the fly ash are responsible for a change in the PZC of the composites.

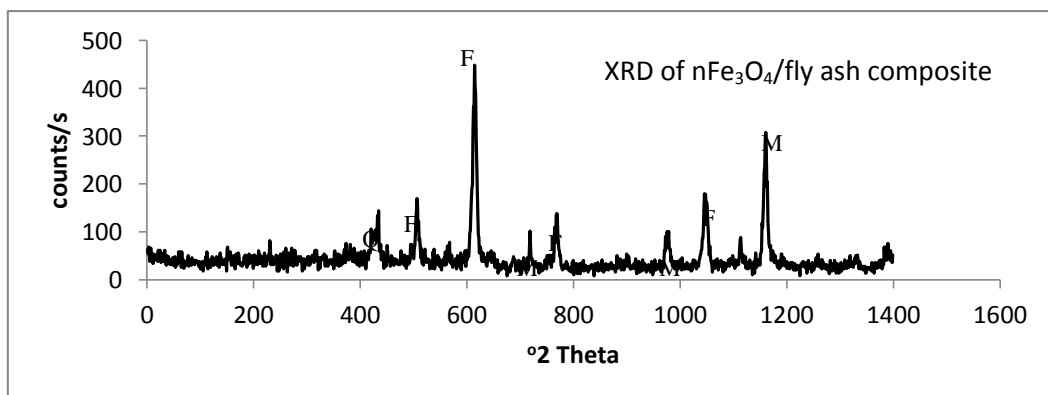
When the pH is lower than the PZC value, the acidic water donates more protons than hydroxide groups and hence the adsorbent surface is positively charged (attracting anions). Conversely, if the pH is above the PZC, the surface is negatively charged and will attract cations or repel anions [22]. Hence, the surface of fly ash, $n\text{Fe}_3\text{O}_4$, $n\text{ZnO}$, $n\text{SiO}_2$ /fly ash composite, and $n\text{Fe}_3\text{O}_4$ /fly ash composite is positively charged and will attract anionic complexes of heavy metals while the surface of $n\text{SiO}_2$ and $n\text{ZnO}$ /fly ash composite is negatively charged and will therefore attract cationic complexes during adsorption processes.

3.5. Ash Content

The ash content of the fly ash, $n\text{Fe}_3\text{O}_4$, $n\text{SiO}_2$, and $n\text{ZnO}$ are $97.4 \pm 0.14 \%$, $97.2 \pm 0.02 \%$, $98.3 \pm 0.07 \%$ and $99.2 \pm 0.14 \%$, respectively, while $89.25 \pm 0.07 \%$, $88.15 \pm 0.07 \%$ and $85.9 \pm 0.01 \%$ are recorded as the ash contents of $n\text{Fe}_3\text{O}_4/\text{fly ash}$, $n\text{SiO}_2/\text{fly ash}$ and $n\text{ZnO}/\text{fly ash}$ composites, respectively. The result shows that the percentage of organic materials present in the fly ash, $n\text{Fe}_3\text{O}_4$, $n\text{SiO}_2$, $n\text{ZnO}$, and $n\text{Fe}_3\text{O}_4/\text{fly ash}$, $n\text{SiO}_2/\text{fly ash}$ and $n\text{ZnO}/\text{fly ash}$ composites are 2.6 %, 2.8 %, 1.7 %, 0.8 %, 10.75 %, 11.85 % and 14.10 %, respectively. The result obtained therefore showed that the precursors have the highest percentage of inorganic components compared to the composite materials.

3.6. X-Ray Diffractometry

We have reported the x-ray diffractogram of fly ash, $n\text{Fe}_3\text{O}_4$, $n\text{SiO}_2$, and $n\text{ZnO}$ [23, 24]. The diffractogram of composites as presented in Fig. 6 thus showed that the $n\text{Fe}_3\text{O}_4/\text{fly ash}$ composite consists of mullite ($\text{Al}_6\text{Si}_2\text{O}_{13}$), quartz (SiO_2) and magnetite (Fe_3O_4). The $n\text{SiO}_2/\text{fly ash}$ composite consists of mullite ($\text{Al}_6\text{Si}_2\text{O}_{13}$), quartz (SiO_2) and cristobalite (SiO_2), while, $n\text{ZnO}/\text{fly ash}$ composite consists of mullite ($\text{Al}_6\text{Si}_2\text{O}_{13}$), quartz (SiO_2) and zinc oxide ($n\text{ZnO}$).



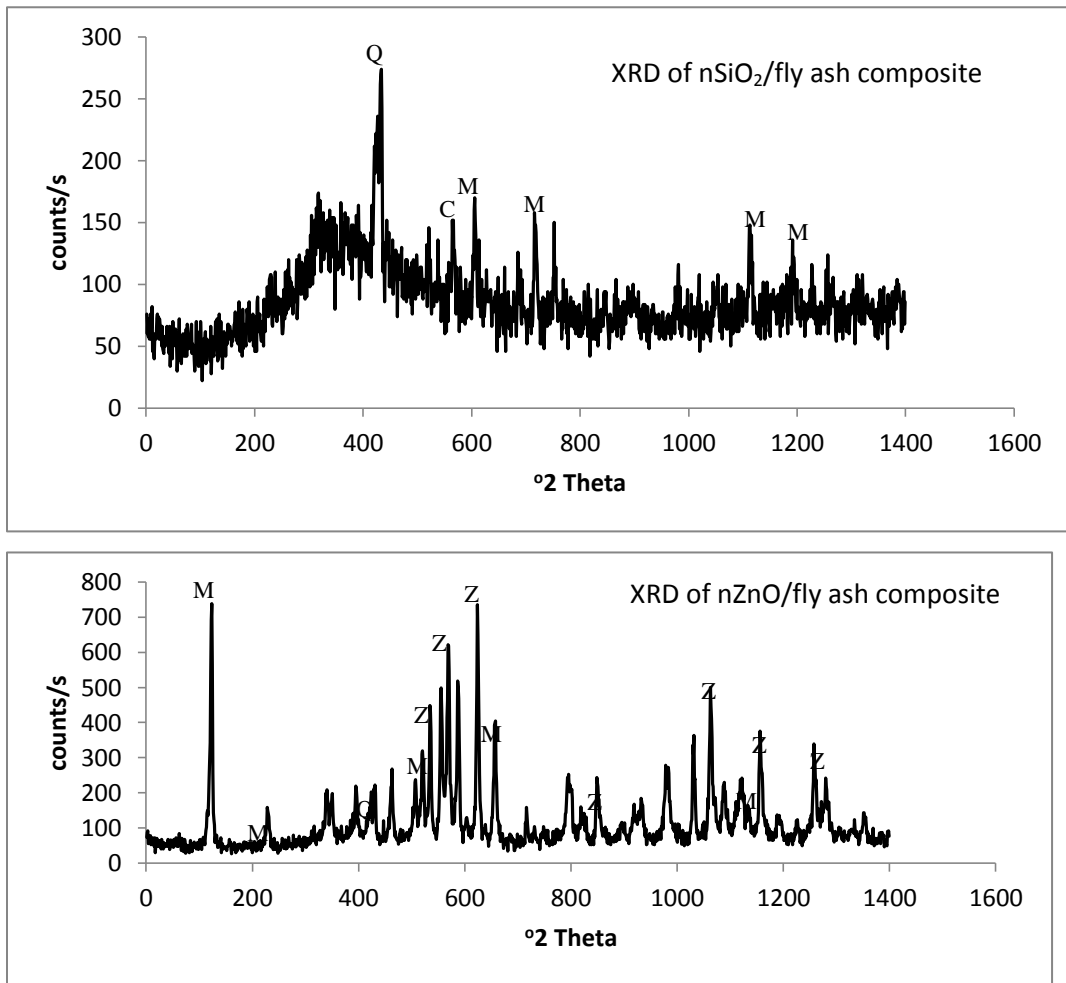


Fig-6. XRD of the composites

M – Mullite ($\text{Al}_6\text{Si}_2\text{O}_{13}$), Q – Quartz (SiO_2), F – Magnetite (Fe_3O_4), C – Cristobalite (SiO_2), Z – Zinc Oxide (nZnO)

The mullite and quartz are from the fly ash, while magnetite, cristobalite and zinc oxide are from the corresponding nano-oxides involved in the composite preparation.

3.7. Surface Area and Micropore Area

The results obtained on the BET surface area and the porosity determination of the composites and the precursors are presented in Table 2. Table 2 shows that the surface area of nFe_3O_4 , nSiO_2 , nZnO and fly ash are 37.18 ± 0.19 , 217.62 ± 1.76 , 14.41 ± 0.0387 and 1.06 ± 0.003 m^2/g , respectively, while the surface area of $\text{nFe}_3\text{O}_4/\text{fly ash}$, $\text{nSiO}_2/\text{fly ash}$ and $\text{nZnO}/\text{fly ash}$ are 207.01 ± 1.20 , 343.75 ± 0.16 and 198.45 ± 0.09 , respectively. The results showed that the use of nano-oxides in the preparation of nano-oxide/fly ash composites greatly accelerated the surface area of fly ash. The surface area of fly ash was therefore increased by 99.49 % for $\text{nFe}_3\text{O}_4/\text{fly ash}$, 99.69 % for $\text{nSiO}_2/\text{fly ash}$ and 99.47 % for $\text{nZnO}/\text{fly ash}$ composites.

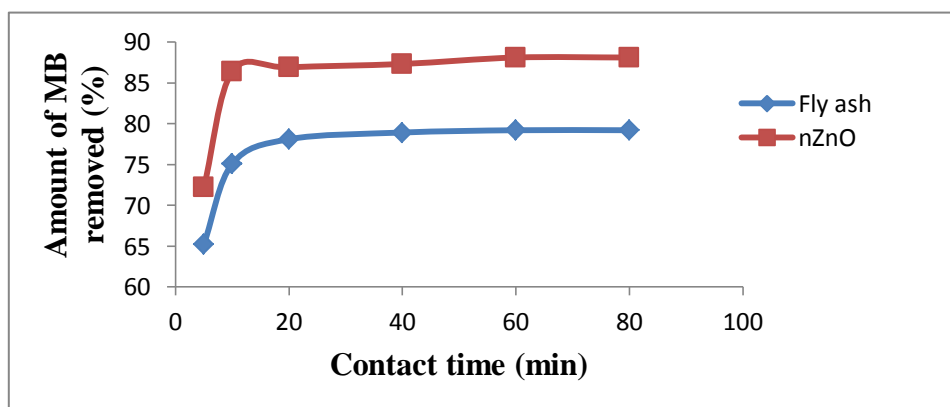
Table-2. BET results of precursors and nano-oxides/fly ash composite materials.

Adsorbents	BET Surface area m^2/g	Micropore Volume cm^3/g	Micropore Area m^2/g	External Surface Area m^2/g	Average pore Diameter Å
Fly ash	1.06 ± 0.003	0.00016	0.38	0.68	89.43
nFe_3O_4	37.18 ± 0.19	0.0017	3.98	33.20	217.42
nSiO_2	217.62 ± 1.76	0.0060	16.13	201.50	88.08
nZnO	14.41 ± 0.04	0.0014	3.18	11.23	98.50
$\text{nFe}_3\text{O}_4/\text{fly ash}$	207.01 ± 1.20	0.085	209.41	197.60	50.99
$\text{nSiO}_2/\text{fly ash}$	343.75 ± 0.16	0.057	35.21	414.97	148.93
$\text{nZnO}/\text{fly ash}$	198.45 ± 0.094	0.002	5.44	73.72	74.10

The micropore area of $\text{nFe}_3\text{O}_4/\text{fly ash}$ was $209.41 \text{ m}^2/\text{g}$; of $\text{nSiO}_2/\text{fly ash}$ it was $35.21 \text{ m}^2/\text{g}$ and of $\text{nZnO}/\text{fly ash}$ it was $5.44 \text{ m}^2/\text{g}$. The micropore areas of fly ash, nFe_3O_4 , nSiO_2 , and nZnO were 0.38, 3.98, 16.13 and $3.18 \text{ m}^2/\text{g}$, respectively, and were thus smaller than the micropore area of the corresponding composites. This shows that the composition of nano-oxides with fly ash also increased the micropore area of fly ash.

3.8. Methylene Blue Adsorption Efficiency and Kinetics

Adsorption kinetics describes the rate of adsorbate uptake governing the contact time of adsorption reaction, which is an important characteristic defining the efficiency of adsorption. It was observed that the adsorption of MB increased steadily in the first 10-20 minutes for all the materials before it slowed down and approached equilibrium.



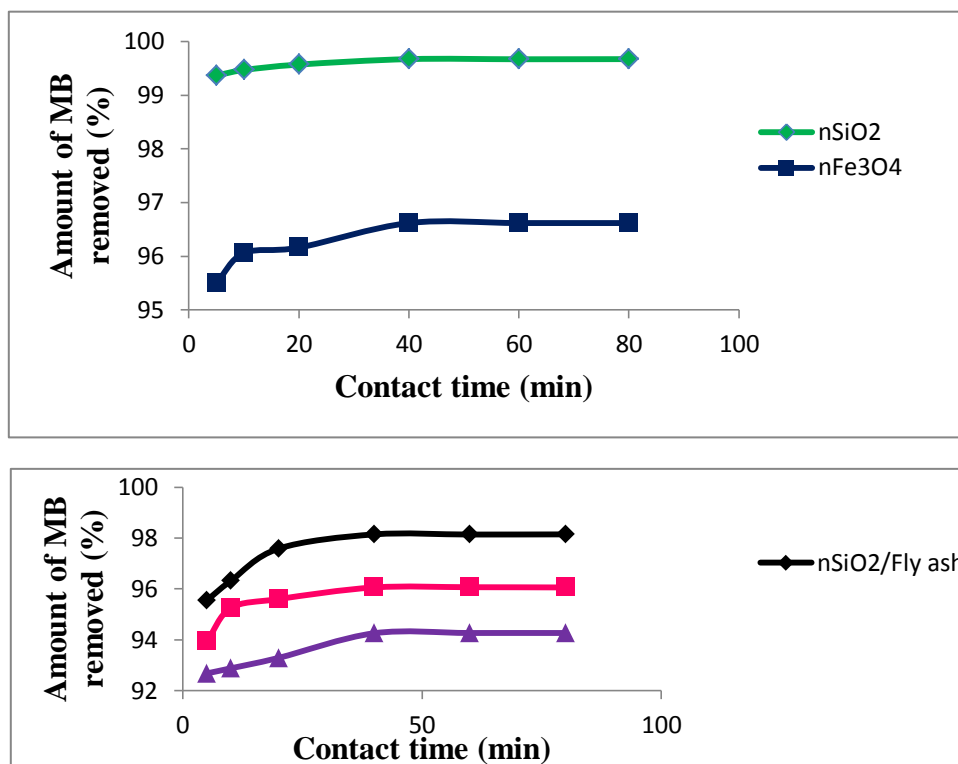


Fig-7. Methylene blue removal efficiencies of the precursors and composites.

Experimental conditions: MB concentration = 10 mg/L; MB solution volume = 100 mL, mass of adsorbent = 0.5 g; stirring speed = 200 rpm, temperature = 20 °C

As can be seen in Fig. 7, approximately 80.9 %, 96.6 %, 99.6 %, 88.9 %, 97.1 %, 98.6 %, and 94.3 % MB were removed from 100 mL of 10 mg/L MB aqueous solution using 0.5 g adsorbents during a contact time of 80 min, stirring speed 200 rpm and a temperature of 20°C, by the fly ash, nFe₃O₄, nSiO₂, nZnO, nFe₃O₄/fly ash, nSiO₂/fly ash and nZnO/fly ash composite, respectively. The order of the decreasing adsorption efficiency of the precursors was: nSiO₂ > nFe₃O₄ > nZnO > fly ash, while the decreasing adsorption efficiency of the composites was: nSiO₂/fly ash > nFe₃O₄/fly ash > nZnO/fly ash. The amount of MB removed by these adsorbents shows that surface area plays a significant role in adsorption. The order of MB removal corresponds to the surface area of precursors and the composites presented in Table 2. During adsorption, pollutants are removed by accumulation at the interface between the adsorbent and the liquid phase; the adsorbing capacity of the adsorbent is at many times associated with the high surface area per unit volume. The calculated value pseudo-second order equation constants are given in Table 3.

Table-3. Pseudo-second order kinetic model parameters for MB adsorption

	Pseudo second-order	Parameters
Fly ash	Equation	$y = 0.6104x + 0.6938$
	q_e (mg/g)	1.6383
	h_0 (mg/g/min)	1.4413
	k_2 (g/mg/min)	0.5370
	R^2	0.9999
nFe ₃ O ₄	Equation	$y = 0.517x + 0.0383$
	q_e (mg/g)	1.9342
	h_0 (mg/g/min)	26.109
	k_2 (g/mg/min)	6.9791
	R^2	0.9999
nSiO ₂	Equation	$y = 0.5015x + 0.01$
	q_e (mg/g)	1.9940
	h_0 (mg/g/min)	100.00
	k_2 (g/mg/min)	25.150
	R^2	0.9999
nZnO	Equation	$y = 0.557x + 0.4617$
	q_e (mg/g)	1.7953
	h_0 (mg/g/min)	2.1660
	k_2 (g/mg/min)	0.6720
	R^2	0.9999
nFe ₃ O ₄ /fly ash	Equation	$y = 0.5165x + 0.1061$
	q_e (mg/g)	1.9361
	h_0 (mg/g/min)	9.4251
	k_2 (g/mg/min)	2.5144
	R^2	0.9999
nSiO ₂ /fly ash	Equation	$y = 0.506x + 0.1172$
	q_e (mg/g)	1.9763
	h_0 (mg/g/min)	8.5324
	k_2 (g/mg/min)	2.1846
	R^2	0.9999
nZnO/fly ash	Equation	$y = 0.5921x + 0.1006$
	q_e (mg/g)	1.6889
	h_0 (mg/g/min)	9.9403
	k_2 (g/mg/min)	3.4849
	R^2	0.9999

It can be seen that the correlation coefficient (R^2) of the pseudo-second order model is high (0.9999) for all the materials. In addition, the calculated q_e values for the pseudo-second order is highly matched with the experimental data, thus, the model suitably predicts the kinetics of MB adsorption onto the precursors and the composites in the current study. This is supported by the work by Chia, et al. [25] and Lin, et al. [26] who reported methylene blue adsorption onto graphene oxide and fly ash, respectively.

4. CONCLUSION

In conclusion, values obtained for the PZC and pH showed that the pH of fly ash, nFe₃O₄, nZnO, nSiO₂/fly ash and nFe₃O₄/fly ash composites are slightly lower than the PZC values, these showing that the surfaces of these materials are positively charged and will attract anionic

complexes of heavy metals in wastewaters. The pH values of nSiO₂ and nZnO/fly ash composites are slightly lower than their PZC values, hence the surface of nSiO₂ and nZnO/fly ash are negatively charged and will attract cationic complexes. The ash content determination also showed that the level of inorganic materials present in the composite materials is a function of the precursors that make up the composite. The BET analysis showed that the composition of nano-oxides with fly ash increased the surface and micropore areas of fly ash which make the composites a better adsorbent than the precursors. Lastly, the adsorption kinetics of MB onto the precursors and composites could well fit into the pseudo second-order model with a good correlation coefficient ($R^2 = 0.9999$). More than 80 % MB was removed by these materials; hence, fly ash produced during the combustion of coal, nano-oxides and composites may be utilized for the remediation of other organic pollutants from wastewaters.

REFERENCES

- [1] Z. Jing, N. Matsuoka, F. Jin, N. Yamasaki, K. Suzuki, and T. Hashida, "Solidification of coal fly ash using hydrothermal processing method. A novel method of advanced materials processing," *J. Mater. Sci.*, vol. 41, pp. 1579-1584, 2006.
- [2] X. Querol, N. Moreno, J. C. Umana, A. Alastuey, E. Hernandez, A. Lopez-Soler, and F. Plana, "Synthesis of zeolites from coal fly ash: An overview," *Int. J. Coal Geol.*, vol. 50, pp. 413-423, 2002.
- [3] S. Wang, "Application of solid ash based catalysts in heterogeneous catalysis," *Environ. Sci. Technol.*, vol. 42, pp. 7055-7063, 2008.
- [4] D. C. D. Nath, S. Bandyopadhyay, P. Boughton, A. Yu, D. Blackburn, and C. White, "High strength biodegradable poly(Vinyl Alcohol)/fly ash composite films," *J. Appl. Polym. Sci.*, vol. 117, pp. 114-121, 2010.
- [5] D. C. D. Nath, S. Bandyopadhyay, J. Campbell, A. Yu, D. Blackburn, and C. White, "Surfacecoated fly ash reinforced biodegradable poly(Vinyl Alcohol) composite films: Part 2-analysis and characterization," *Appl. Surf. Sci.*, vol. 257, pp. 1216-1221, 2010.
- [6] R. Juan, S. Hernandez, X. Querol, J. M. Andres, and N. Moreno, "Zeolite material synthesized from fly ash: Use as cationic exchanger," *J. Chem. Technol. Biotechnol.*, vol. 77, pp. 299-304, 2002.
- [7] P. R. Penilla, A. G. Bustos, and S. G. Elizalde, "Immobilization of Cs, Cd, Pb and Cr by synthetic zeolites from Spanish low-calcium coal fly ash," *Fuel*, vol. 85, pp. 823-832, 2006.
- [8] P. K. Rohatgi, N. Gupta, and S. Alaraj, "Thermal expansion of aluminum-fly ash cenosphere composites synthesized by pressure infiltration technique," *J. Compos. Mater.*, vol. 40, pp. 1163-1173, 2006.
- [9] O. M. Dunens, K. J. Mackenzie, and A. T. Harris, "Synthesis of multiwalled carbon nanotubes on fly ash derived catalysts," *Environ. Sci. Technol.*, vol. 43, pp. 7889-7894, 2009.
- [10] C. N. Panagopoulos, E. P. Georgiou, A. Tsopani, and L. Piperi, "Composite ni-co-fly ash coatings on 5083 aluminium alloy," *Appl. Surf. Sci.*, vol. 257, pp. 4769-4773, 2011.
- [11] A. Papandreou, C. J. Stournaras, and D. Panias, "Copper and cadmium adsorption on pellets made from fired coal fly ash," *J. Hazard. Mater.*, vol. 148, pp. 538-547, 2007.
- [12] S. Wang, Q. Ma, and Z. H. Zhu, "Characteristics of coal fly ash and adsorption application," *Fuel*, vol. 87, pp. 3469-3473, 2008.

- [13] N. Nascimento, P. S. M. Soares, and V. P. Souza, "Adsorption of heavy metal cations using coal fly ash modified by hydrothermal method," *Fuel*, vol. 88, pp. 1714-1719, 2009.
- [14] L. Wei, K. Wang, Q. Zhao, C. Xie, W. Qiu, and T. Jia, "Kinetics and equilibrium of adsorption of dissolved organic matter fractions from secondary effluent by fly ash," *J. Environ. Sci.*, vol. 23, pp. 1057-1065, 2011.
- [15] O. S. Fatoki, O. S. Ayanda, F. A. Adekola, and B. J. Ximba, "Sorption of triphenyltin chloride to nFe₃O₄, fly ash and nFe₃O₄/fly ash composite material in seawater," *Clean – Soil, Air, Water*, vol. 42, pp. 472 - 479, 2014.
- [16] O. S. Ayanda, O. S. Fatoki, F. A. Adekola, and B. J. Ximba, "Utilization of nSiO₂, fly ash and nSiO₂/fly ash composite for the remediation of triphenyltin (TPT) from contaminated seawater," *Environ. Sci. Pollut. Res.*, vol. 20, pp. 8172-8181, 2013.
- [17] S. W. Oh, M. N. Kang, C. W. Cho, and M. W. Lee, "Detection of carcinogenic amines from dyestuffs or dyed substrates," *Dyes Pigments*, vol. 33, pp. 119 -135, 1997.
- [18] K. S. Wang, M. C. Wei, T. H. Peng, H. C. Li, S. J. Chao, T. F. Hsu, H. S. Lee, and S. H. Chang, "Treatment and toxicity evaluation of methylene blue using electrochemical oxidation, fly ash adsorption and combined electrochemical oxidation-fly ash adsorption," *J. Environ. Manage.*, vol. 91, pp. 1778-1784, 2010.
- [19] A. M. M. Vargas, A. L. Cazetta, M. H. Kunita, T. L. Silva, and V. C. Almeida, "Adsorption of methylene blue on activated carbon produced from flamboyant pods (*Delonix Regia*): Study of adsorption isotherms and kinetic models," *Chem. Eng. J.*, vol. 168, pp. 722-730, 2011.
- [20] F. Adekola, M. Fédoroff, H. Geckeis, T. Kupcik, G. Lefèvre, J. Lützenkirchen, M. Plaschke, T. Preocanin, T. Rabung, and D. Schild, "Characterization of acid-base properties of two gibbsite samples in the context of literature results," *J. Colloid and Interface Sci.*, vol. 354, pp. 306-317, 2011.
- [21] D. Gianina, M. Crisan, M. Zaharescu, N. I. Ionescu, and M. Rusu, "TEM micrographs fractal analysis." Available <http://isis.pub.ro/iafa2003/files/5-1.pdf> [Accessed: 29/05/2011], 2003.
- [22] Y. Zheng, J. Zhang, and A. Wang, "Fast removal of ammonium nitrogen from aqueous solution using chitosan-g-poly(Acrylic Acid)/attapulgitic composite," *Chem. Eng. J.*, vol. 155, pp. 215-222, 2009.
- [23] O. S. Fatoki, O. S. Ayanda, F. A. Adekola, B. J. Ximba, and B. O. Opeolu, "Preparation and characterization of activated carbon - nFe₃O₄, activated carbon - nSiO₂ and activated carbon - nZnO hybrid materials," *Part. Part. Syst. Charact.*, vol. 29, pp. 178 - 191, 2012.
- [24] O. S. Ayanda, S. Fatoki, F. A. Adekola, and B. J. Ximba, "Characterization of fly ash generated from matla power station in mpumalanga, South Africa," *E-J Chem.*, vol. 9, pp. 1788 - 1795, 2012.
- [25] C. H. Chia, N. F. Razali, M. S. Sajab, S. Zakaria, N. M. Huang, and H. N. Lim, "Methylene blue adsorption on graphene oxide," *Sains Malaysiana*, vol. 42, pp. 819-826 2013.
- [26] J. X. Lin, S. L. Zhan, M. H. Fang, X. Q. Qian, and H. Yang, "Adsorption of basic dye from aqueous solution onto fly ash," *J. Environ. Manage.*, vol. 87, pp. 193-200, 2008.

Views and opinions expressed in this article are the views and opinions of the author(s), International Journal of Chemistry and Materials Research shall not be responsible or answerable for any loss, damage or liability etc. caused in relation to/arising out of the use of the content.